AIMS Geosciences, 10(1): 47–61.
DOI: 10.3934/geosci.2024004
Received: 19 July 2023
Revised: 12 December 2023
Accepted: 08 January 2024
Published: 24 January 2024

http://www.aimspress.com/journal/geosciences

Research article

Applications of the scanning test of trend changes in regression coefficients to monthly temperature over China and Globe

Jianmin Jiang[1,2,*]

[1] Key Laboratory of Desert and Desertification, Chinese Academy of Sciences, Lanzhou 730000, China
[2] China Meteorological Administration Training Centre, Beijing 100081, China

* **Correspondence:** Email: jmjiangjm@foxmail.com; Tel: 86-17800814497.

Abstract: The algorithm of the scanning t-test of regression slope-coefficients in two phases is introduced to detect trend change-points, along with a coherency analysis of changes between two time series. This new algorithm is different from the previously published scanning F_{max} test of trend changes. Meanwhile, the fuzzy weighted moving average (FWMA) was employed to intuitively verify the results of segment regressions. Then, these algorithms were applied to two series of monthly temperature over mainland China and the globe for January 1901–December 2020. The applied results show that significant changes in segment trends may be classified into two gradations on interdecadal and intradecadal scales. The coherency of trend changes between the two series were mostly positive, with a few differences in the change dates. The global warming "hiatus" was detected as two processes on the intradecadel scale: a sharp droop-down from July 1998 to February 2000 following a short warming up; the second weaker droop-down happened from November 2003 to July 2009. Thus, it was featured on the interdecadel scale as the warming rate slowed down to be nearly stable from October 2002 to June 2009 in globally but without turning into cooling. Mainland China seemed to slow down weaker, but lasted longer than the globe. A somewhat unexpected finding is that the warming rate over Mainland China was lower than that for the globe in the case of standardized differences. This contradicts the previous conclusion that resulted from annual anomalies of temperature. It is suggested that the anomalies in the distribution *N(0,s)* might be referred to the "perceptual" index to compare variations in the same series or between two series but with the same variance and distribution, while referring to the standardized differences in *N(0,1)* as a "net" indicator to compare fluctuations between two series with different variances, even in different distributions.

Keywords: algorithm of scanning test; trend change; regression coefficient; coherency; globe; China mainland; fuzzy weighted moving average

1. Introduction

Research of change point been of interest for many years in a wide range of scientific fields. For example, for global warming, Varotsos et al. [1,2] and Jones and Ricketts [3] reported abrupt step-like changes of the segment average in global tropospheric temperature and SST (sea surface temperature), among many previous publications.

Jiang published a monograph [4] in 2021 and introduced five algorithms, which include the scanning tests of detecting change points in the subsample mean, variance, trend, and correction between two series, along with coherency analysis for a pair of series in detail. It also described practical applications to time series of monthly temperature in mainland China and across the globe, of hydrology and precipitation, and of tree ring chronology respectively.

One of the five algorithms, the scanning F_{max} test, was developed to detect trend changes. This was extended from a review paper by Lund and Reeves [5] who originally detected only one change point in subsample means with the regressive step coefficient $\boldsymbol{a}$. The test index in the F_{max} test was based on the difference of the sum of squared regression error (SSE) between two-phase models and the pooled one-phase regression. In a subsequent study, it was found that their index can also test indirectly the trend indicated by the slope coefficient $\boldsymbol{b}$ in regression models [4,6,7].

This paper introduces a different scanning t-test algorithm of directly detecting the regressive slope coefficients to reveal trend changes, and we also carry out a coherency analysis. It can be applied for comparing and estimating segment trend rate in climate warming or cooling. The application was performed on two series of monthly temperature over mainland China and the globe for the period spanning 1901–2022, because the F_{max} test failed to be applied to these two series. They were spatially averaged over large area of China or the globe resulting in too high of a serial dependence that is beyond the F_{max} test's strict Mont-Carlo correction.

Section 2 briefly introduces methodologies of this new algorithm, a fuzzy weighted moving average (FWMA), and the data source. The application results are described in Section 3, in which the FWMA is used for intuitively verifying the resulting regressive models. Section 4 discusses why global warming in China was weaker than that across the globe in the case of standardized differences, which is in contrast to the conclusion from the anomaly series. A summary is presented in Section 5.

2. Methods and materials

2.1. Algorithm of the scanning t-test of trend change points

This subsection briefly introduces the scanning t-test of the regressive slope coefficient [8].

Supposing two phase linear regression models in a time series x_j (j = 1, 2, 3, …, j, …, J), the two subsample regression models may be written as

$$\hat{x} = a_{j1} + b_{j1}t + \varepsilon, \quad \hat{x} = a_{j2} + b_{j2}t + \varepsilon \text{ , and}$$

$$\hat{x} = a_{j0} + b_{j0}t + \varepsilon \quad \text{for one phase joining the } j1 \text{ and } j2 \tag{1}$$

where *j1* denotes a subsample before the reference point *j*, while *j2* indicates the subsample after *j* with the same size *n*. *t = 1, 2, ..., j, ..., J.*

Modifying the sampling test of the regression coefficient [9,10], the statistics of the scanning *t*-test are then formulated for subsample size *n = 2, 3, ..., < J/2* and reference points *j = n+1, n+2, ..., J-n*.

$$T_b(n,j) = \left[\frac{S_{tj0}\sqrt{n-2}}{S_{xj0}\sqrt{1-r_{j0}^2}}(b_{j2}-b_{j1})\right] \Big/ T_\alpha(n-2) \tag{2}$$

where b_{j2} denotes the regressive slope coefficient of the subsample after *j,* while b_{j1} indicates that before *j* in same size *n*. S_{tj0}^2 represents the variance of variable *t* in the pooled subsample joining *j1* and *j2*, i.e.

$$S_{tj0}^2 = \frac{1}{2n-1}\sum_{i=j-n}^{j+n-1}\left(t_i - \overline{t_{j0}}\right)^2 \tag{3}$$

On the other hand, S_{xj0}^2 is the variance of variable x for the pooled subsample:

$$S_{xj0}^2 = \frac{1}{2n-1}\sum_{i=j-n}^{j+n-1}\left(x_i - \overline{x_{j0}}\right)^2 \tag{4}$$

The parameter r_{j0} in (2) denotes the correlation coefficient of the variable x with respect to t in the pooled subsample:

$$r_{j0} = \frac{\sum_{i=j-n}^{i=j+n-1}\left(x_i - \overline{x_{j0}}\right)\left(t_i - \overline{t_{j0}}\right)}{\left[\sum_{i=j-n}^{i=j+n-1}\left(x_i - \overline{x_{j0}}\right)^2 \times \sum_{i=j-n}^{i=j+n-1}\left(t_i - \overline{t_{j0}}\right)^2\right]^{1/2}} \tag{5}$$

Setting *m=0: ms= j − n and me=j+n-1 for the pooled subsample joining j1 and j2,*

m=1: ms= j − n and me=j-1, for subsample j1 before the reference point j,

m=2: ms=j and me=j+n-1, for subsample j2 after j.

The parameters a_{jm} and b_{jm} are the same as in [4,6,7]. Here, they are repeated for convenience to readers:

$$a_{jm} = \overline{x_{jm}} + b_{jm}\overline{t_{jm}} \tag{6}$$

$$b_{jm} = \frac{\sum_{i=ms}^{me}(t_i - \overline{t}_{jm})(x_i - \overline{x}_{jm})}{\sum_{i=ms}^{me}(t_i - \overline{t}_{jm})^2} \tag{7}$$

where $\overline{t_{jm}}$ and $\overline{x_{jm}}$ are the subsample means of variables *t* and *x*, respectively:

$$\overline{t_{jm}} = \frac{1}{(me-ms)}\sum_{i=ms}^{i=me} t_i \tag{8}$$

$$\overline{x_{jm}} = \frac{1}{(me-ms)}\sum_{i=ms}^{i=me} x_i \tag{9}$$

Theoretically, the $T_b(n,j)$ is in the Student's t distribution. In its two-dimensional contour map, a local positive maximum center with $T_b(n,j) > 1.0$ denotes a change point to start an increasing trend, while a local negative minimum center with $T_b(n,j) < -1.0$ indicates a change point to start a decreasing trend.

The coherency index of trend changes between the globe (l) and China (s) is calculated as follows [6,7]:

$$T_{bc}(n,j) = \frac{T_{bl}(n,j) \times T_{bs}(n,j)}{|T_{bl}(n,j) \times T_{bs}(n,j)|^{1/2}} \tag{10}$$

Similarly, in its two-dimensional contour map, the local maximum center with $T_{bc}(n,j) > 1.0$ suggests an in-phase trend change, whereas the local minimum center with $T_{bc}(n,j) < -1.0$ indicates an out-of-phase trend change between the two series if at least one local center in $T_{bl}(n,j)$ or $T_{bs}(n,j)$ matches. If a coherency local center does not match with any local center in the series, this might indicate some change-point dating or trend-slope differences between the two series. The particular trend in each series depends upon the fitted line of the linear regression.

In practice, one may select a suitable interval on n or j to reduce the resolution of the scanning t-test.

2.2. Algorithm of the fuzzy weighted moving average (FWMA)

The moving average or low-pass filter has been employed widely in various scientific and social fields. However, users often leave blanks [11–15] or set just a constant of average [16] at the beginning and end points without calculation, especially in the study of climate change. To reduce the data boundary influence in computation, the author coded a computing program of the FWMA as follows [8,17]:

$$\widetilde{x_j} = \begin{cases} \dfrac{\sum_{i=1}^{i=j+\frac{K}{2}} G(k)x(i)}{\sum_{i=1}^{i=j+\frac{K}{2}} G(k)}, & for\ 1 < j < \frac{K}{2}, \\ \dfrac{\sum_{i=j-\frac{K}{2}}^{i=j+\frac{K}{2}} G(k)x(i)}{\sum_{i=j-\frac{K}{2}}^{i=j+\frac{K}{2}} G(k)x(I)}, & for \frac{K}{2} < j < \left(J - \frac{K}{2}\right), \\ \dfrac{\sum_{i=j-\frac{k}{2}}^{i=J} G(k)x(i)}{\sum_{i=j-\frac{k}{2}}^{i=J} G(k)}, & for\ (J - K/2) < j < J\ . \end{cases} \tag{11}$$

where $G(k)$, $(k = 1, 2, ..., K << J)$, denotes a K-point Gaussian function and as the weightings, $k = i-j+1+K/2$, $K/2 = INT(K/2)$. The odd number K for $G(k)$ is the calculating window. The middle formula is equivalent to the low-pass filter for the middle part of the series to be calculated, because the denominator equals 1.0. The formula equals a moving average when $G(k) = 1/K$ at every point. Of course, the weight function $G(k)$ may be taken in other ways, even the denominator does not equal 1.0.

Theoretically, formula (11) agrees with the fuzzy weighted average (FWA) method, which was proposed initially by Baas and Kwakernaak [18], and then has been widely discussed in the context

of fuzzy systems [19,20] with different subscript indices. Here, particular subscript indexes have been coded directly for practical computation.

2.3. Data source

The monthly anomalies of temperature across the globe for 1850–2022 were downloaded from the website https://crudata.uea.ac.uk/cru/data/temperature/, with file name HadCRUT5. It was modified and updated by Morice et al. [21]. The dataset consists of monthly anomalies relative to the monthly average over 30 years (1961–1990). These average values over 1961–1990 were commonly used as the climatologic baseline in IPCC [22]. The spatial resolution of the data is 5° log. × 5° lat. per grid box.

The dataset of monthly temperature for mainland China was downloaded from http://www.cru.uea.ac.uk/cru/data/hrg/ with file name CRU CY. The spatial resolution in this file is 0.5° log. × 0.5° lat. per grid box, which is a much higher resolution than the HadCRUT5. It contains 287 files for countries or regions. The 55th file is for mainland China covering the years of 1901–2022 [23].

In this work, the two series were normalized with respect to the monthly data to remove the differences and effects of seasonal cycles. That is, each series was variance-adjusted from their monthly anomalies into their monthly standardized differences by dividing the corresponding monthly climatologic standard deviation. The standard deviation is another statistical parameter of the climatologic variance [22] relative to the same baseline period.

3. Results from the scanning t-test

The results of this scanning t-test were produced by computing Eqs. (2–9) at a confidence level of $\alpha = 0.01$. Because the two series were monthly averaged spatio-temporally over mainland China and the globe, so that the two series are apparently in serial dependence. Thus, the computed results of $T_b(n,j)$ are far larger than 1.0 in most cases with different magnitudes to each other. This leads to difficulties in setting the test threshold, and the coherency might depend upon one side of the large magnitude. In order to improve plotting, considering that the change points are detected by the local centers in a relativity to around grids, we tried to transfer every value of $T_b(n,j)$ into the plotting values, by proportionally dividing a quasi-standard deviation as follows:

$$\hat{\mathrm{T}}_b(n,j) = \mathrm{T}_\mathrm{b}(n,j) \Big/ \left[\frac{1}{N \times K} \sum_{j=1}^{j=N} \sum_{k=1}^{k=K} \mathrm{T}_\mathrm{b}(n_k, j)^2\right]^{1/2} \tag{12}$$

The denominator is just a proportion coefficient without modifying the zero line and contour's pattern. The threshold may be chosen from the Student distribution form in books besides 1.0.

Then, the contours of $\hat{T}_b(n,j)$ for mainland China, the globe and their coherency are plotted in Figures 1b, 2b, and 3b, separately. Figures 1a, 2a, and 3a illustrate the fitted regression lines, i.e. the $\hat{x}$ in Eq. (1) on interdecadal scales, which are mostly for scales >120 months. Figures 1c, 2c, and 3c show regression lines on intradecadal scales ≤120 months. Here, the inter- or intra-decadal scales represent a persistent trend segment but not a cycle of oscillation.

3.1. Change points and segment regressions for mainland China

After comparison of this downloaded data with observed data for mainland China, Jiang [17] illustrated that the annual anomalies of the downloaded dataset that is also used here, are usually lower than the observed values of the average over 160 basic meteorological stations in mainland China, but the change trends are in agreement with each other. For example, the warmest year is in 2021 for both, but the downloaded value was 8.50 ℃ compared to the observed record 10.53 ℃ [24]. Both had a reduction of a little in 2022 from 2021, but with different values: 8.30 ℃ in downloaded and 10.51 ℃ in the observed dataset [24]. However, the observed dataset begins in 1951. So, the downloaded data are used in this work for detecting change trends for longer periods.

The contour patterns of $\hat{T}_b(n,j)$ for mainland China was plotted as Figure 1b. It is obvious that the centers appear in two categories on the contour map: interdecadal scales and intradecadal scales. The physical background was tested and discussed in [3]. There are five local centers on the interdecadal scales. The first center was positive in June 1915 on a time scale of 169 months; the second center was negative in May 1940 on a 446-month scale; and the third center was positive in August 1973 on the scale of 588-months. This was then followed by a negative change in July 2002 on a 128 month scale. The last center in August 2014 on a 97 month scale was slightly low because of the nearby ending of the series.

On the intradecadal scales, there are 19 small centers. They were significant except for four centers around 1912, 1915, 1924, and 1935, as shown in Figure 1b.

The linear regression models were calculated following Eq (1) to fit every segment data between two neighbor points. Subsequently, the regression lines $(\hat{x})$ for all segments are plotted as thick solid lines in Figure 1a. It illustrates six linear regressions on interdecadal scales. The earliest subperiod persisted for 173 months (January 1901–May 1915) with slight cooling, followed by a slow warming until April 1940 with a duration of 299 months. The third segment from May 1940 to July 1973 (399 months) was close to the climatologic baseline, but cooling very slowly. China began to warm up rapidly in August 1973 until June 2002. This warming rate is larger than in the second subperiod (Table 1). The next one from July 2002 to July 2014 was a little later than the global warming "hiatus" [25–38], but featured the warming slowdown without trend turning to cooling. After August 2014, it was warming up again, and the warming rate became the largest one among the six episodes (Table 1).

On the intradecadal scales (Figure 1c), twenty segment regressions on short scales are embedded in the interdecadal trend changes. These short scale regressions may be referred to as the climate variations rather than trend changes. A few statistical features are described here, because there were too many subperiods. The subperiod duration varied from 17 months in 1914–1915 to 140 months in 1901–1912. The average duration was 73.2 months. It seems to portray a common feature: the up-down variations were obvious after 1945.

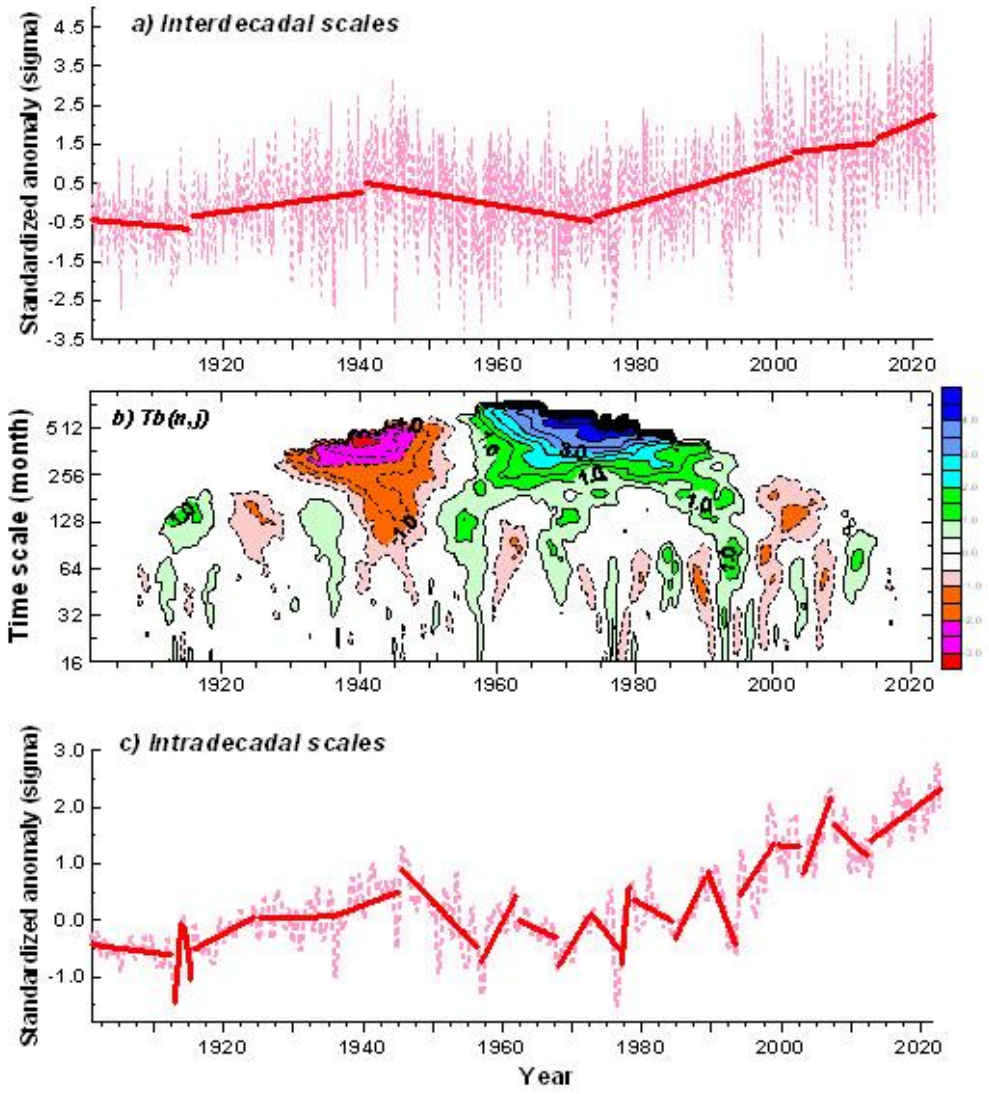

Figure 1. a) Regression models fitted to segment data on interdecadal scales for mainland China. Thick solid red lines indicate regression lines. The thin dashed line in light red denotes the monthly standardized differences. b) Contours of the statistic $\hat{T}_b(n,j)$ resulted from the scanning t-test for mainland China. The contour interval is 0.25, but the contour of zero is not shown. The proportion coefficient is 2.86. c) The same as in (a) but for intradecade scales, the thin dashed curve in light red represents the FWMA at 13-point Gaussian function for monthly standardized differences for intuitively verifying the regressive models.

3.2. Change points and segment regressions globally

Figure 2b depicts the global results. There are four local centers on interdecadal scales with one center less than that for China in the 1910's. The first center is negative in July 1940 on a scale of 446 months; the second center is positive in December 1977 on a 512-month scale; and the third center is negative again in October 2002 on a 128-month scale. The last one in July 2009 on a scale of 97 months is weaker because of the nearby the ending of the series.

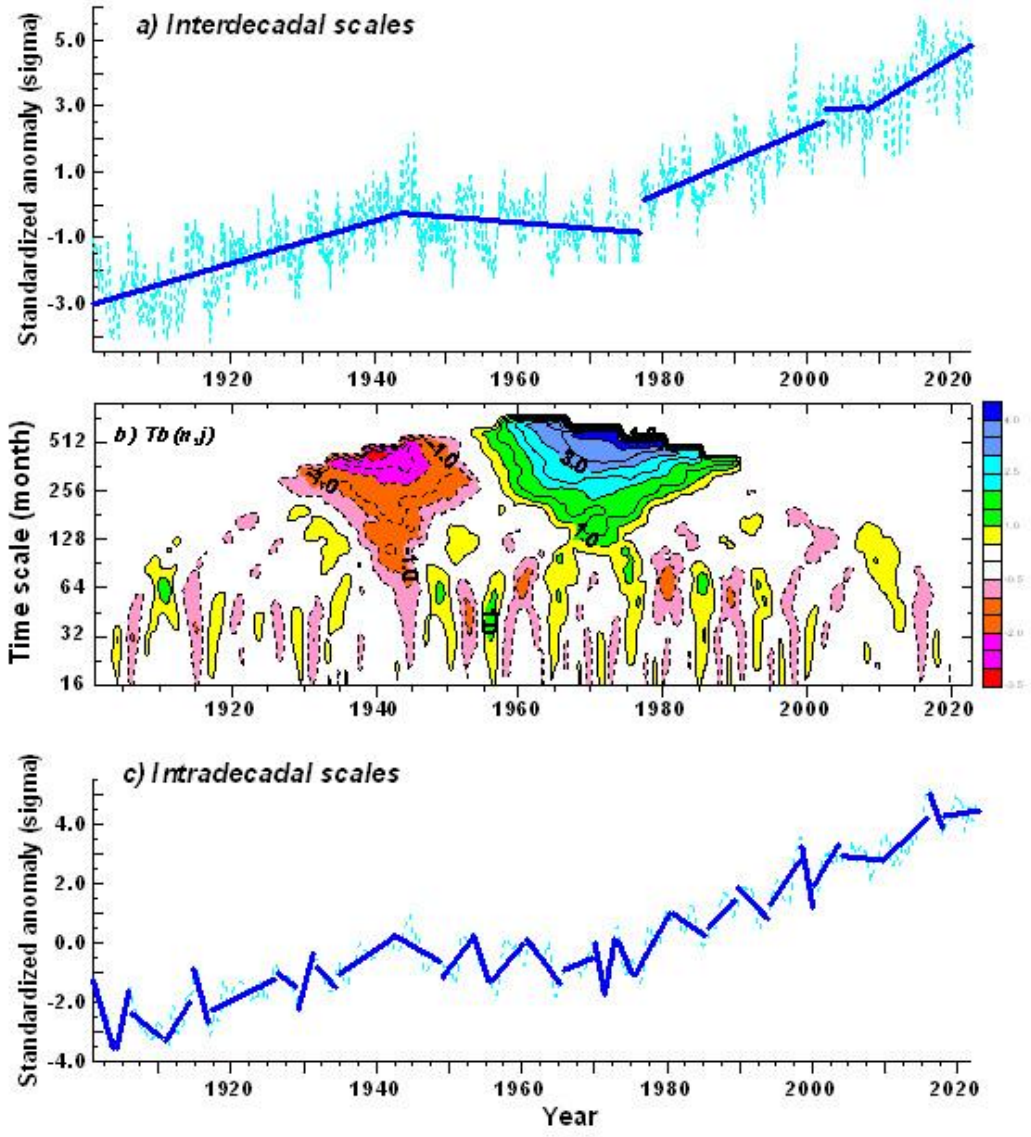

Figure 2. The same as in Figure 1 but for the globe. The proportion coefficient is 5.53.

Figure 2a illustrates five segments on interdecadal scales. Differences from that for China mainly occurred before 1920. The first segment appeared in January 1901–May 1943 (509 months, Table 1) with a warming trend but weaker than that after 1977. The second subperiod from June 1943 to February 1977 (405 months) changed into a cooling trend. The next subperiod from March 1977 to September 2002 (307 months) was the first stage of modern global warming, in which the warming rate was much larger than that before 1943 (Table1). The subperiod between October 2002 and January 2008 warmed up very little. That coincided with the warming "hiatus", which has been argued for years [25–38]. In fact, the data showed that the summer of 1998 was suddenly hot reaching the first peak warming since 1976, and the monthly anomaly in July 1998 reached up to above 0.726 °C relative to July of 1961–1990. But, it suddenly cooled down from August 1998 to February 2000, then it warmed up again but weaker than that before July 1998. The second cooling down happened in a longer period from November 2003 to July 2009 on the intradecadal scale (Figure 2c). The "hiatus" was confirmed by a deceleration of sea level rise derived from satellite-based data [39]. After 2008, global warming came again even stronger than previously. The warming rate increased (Table 1), and

the maximum record occurred in August 2016, and the monthly anomaly reached up to 0.863 ℃ above the baseline for August of 1961–1990, The annual anomaly in 2016 got up to 0.875 ℃ relative to annual of 1961–1990 (HadCRUT5).

There are 29 local centers on the intradecadal scales with eight points more than that in mainland China. Thus, thirty segment regression lines are delineated in Figure 2c. The averaged subperiod duration was 49 months, and varied from 19 months (in December 1969–June 1971) to 108 months (in March 1917–February 1926).

Table 1 Change points, duration, and statistical parameters for every subperiod on interdecadal scale.

Change point in month		Duration (months)		Regression Coefficient b		Correlation Coefficient r	
Globe	China	Globe	China	Globe	China	Globe	China
1901/01↑	1901/01↓	509	173	0.005	−0.001	**0.72**	−0.10
	1915/06↑		299		0.002		0.20
1943/06↓	1940/05↓	405	399	−0.00001	−0.002	−0.22	−**0.25**
1977/03↑	1973/08↑	307	347	0.008	0.004	**0.71**	**0.39**
2002/10↓	2002/07↓	64	145	0.001	0.002	0.03	0.06
2008/02↑	2014/08↑	179	101	0.011	0.006	**0.56**	0.15
2022/12	2022/12						

Note: *$r_{0.01}$=0.32 for n=60; $r_{0.01}$=0.25 for n=100.

For detailed comparison, Table 1 lists the change points in month, subperiod duration, regressive slope coefficient b, and correlation coefficient r for every subsample on interdecadal scales for China and the globe respectively. The last two columns show segment correlation coefficients. The three warming phases for globally, and the longest two segments between 1940 and 2002 in China were significant (black numbers) at a confidence level of $\alpha = 0.01$.

3.3. Coherency analysis

The coherency of trend changes between China and the globe is plotted in Figure 3. In Figure 3b, the contours pattern shows mostly positive coherency, and suggests that most trend changes were in phase between the two series.

Figure 3a copies regression models from Figures 1a and 2a into one panel to illustrate the coherent relationships on interdecadal scales. Figure 3c is the same as in Figure 3a, but on intradecadal scales. It is found that the change trends were mostly agreement between China and the globe (Figure 3a and Table 1). But in the early years before 1915, China was weakly cooling. This difference was not reflected in Figure 2b, probably because the $T_b(n,j)$ is nearly zero for the globe (Figure 2b), corresponding to the first positive center in China. The change points in 1940's and 1970's for mainland China were earlier than that of the globe with a short time of around 3 years only. The global warming "hiatus" was composed of two processes on short scales as mentioned above. However, It showed that a warming slow down with only 0.001σ/month of warming rate for 64 months happened from October 2002 to January 2008 (Table 1) according this detection on the interdecadal scale. Actually, a decline trend of monthly temperature was detected only in the global SST from November 2002 to March 2008 [8]. In China, the warming "hiatus" seemed weaker but lasted longer than globally (Figure 3a, Table 1).

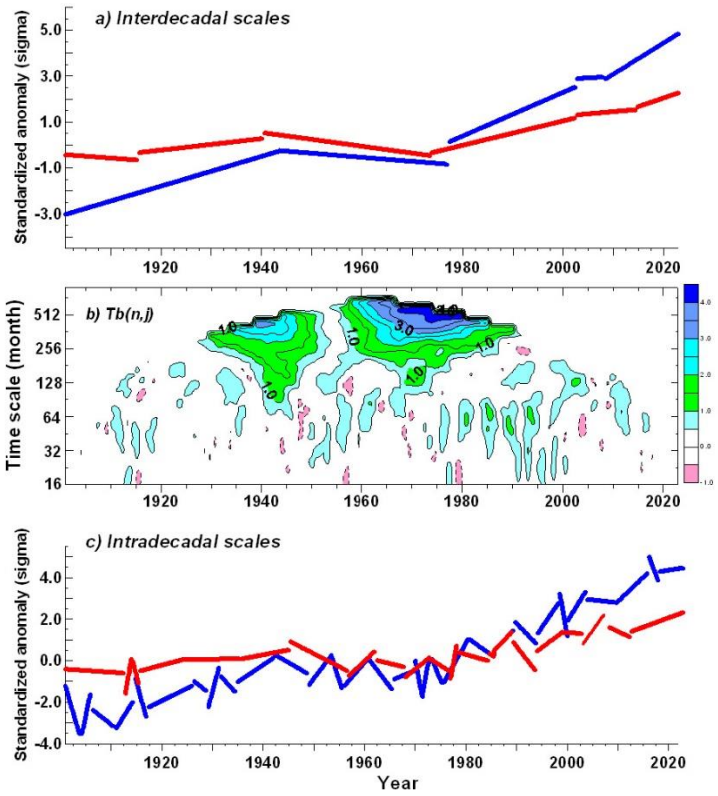

Figure 3. a) Regression models for mainland China (red lines) and the globe (blue lines) on interdecadal scales. b) Same as in Figure 1b, but for coherency between mainland China (Figure 1b) and the globe (Figure 2b). c) The same as in Figure 3a but for intradecadal scales.

A somewhat surprising result was detected here that, in the global warming process, China warmed up more slowly than the globe did in the case of variance-adjusted anomalies (Figure 3a and 3c). That is, contrary to the conclusions resulting from annual anomaly series [14,15]. This finding confirms Jiang's result from the observed average over 160 stations in mainland China [4], despite the data sources being different. The reason, in statistics, will be discussed in the next section.

4. Discussion

This section discusses the statistical reason why the contrasting conclusions of the global warming rate happened between the standardized differences and the anomalies for China and the globe. As is well known, the standardized differences in the probability distribution *N(0,1)* are computed as the anomalies in *N(0,s)* divided by the climatologic standard deviation (SD). Thus, the SD explains why the standardized differences are different from the anomalies. Figure 4 compares the monthly climatologic SD between mainland China (red lines) and the globe (blue lines) based on the baseline period of 30 years (1961–1990). The obvious differences are evidence that the SDs in each month as well as seasonal cycle were much larger in China than that of the globe. This is easy to understand because oceans occupy 70% of the global area, even 77% (1995/2592) of the grid boxes in computation, adding more weight to the global warming index. Sea water's specific heat is 3 times that of air over lands. Ding and Wang [14] did note the ocean roles importance globally, so that using the anomalies to compare the warming rate between China and the globe is not exactly scientific. Yet, the ratios of

the monthly SD of China to the globe were larger in winter than in summer. The minimum ratio of 0.32/0.15 = 2.13 times that of China to the globe occurred in July, while the maximum ratio, 1.32/0.24 = 5.50, happened in February. Larger SD implies a larger variation scope of variance-adjusted anomalies (Figure 5). These statistical results, i.e. that China's climatologic variance is much larger than that of the gobe's, might statistically explain why the anomalies in China experenced warming higher than that of the globe, but the standardized differences in China were inversely showed warming weaker than that of globe. Also, the climatologic variances of both China and the globe in winter were larger than that in summer (Figure 4) which may explain why the warming in winter was much more obvious than that in summer [15,40].

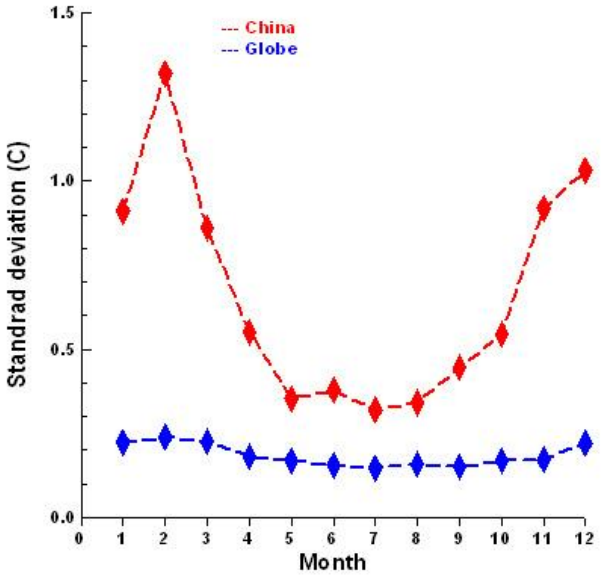

Figure 4. Comparisons of monthly climatologic standard deviation (SD) of temperatures between mainland China (red) and the globe (blue).

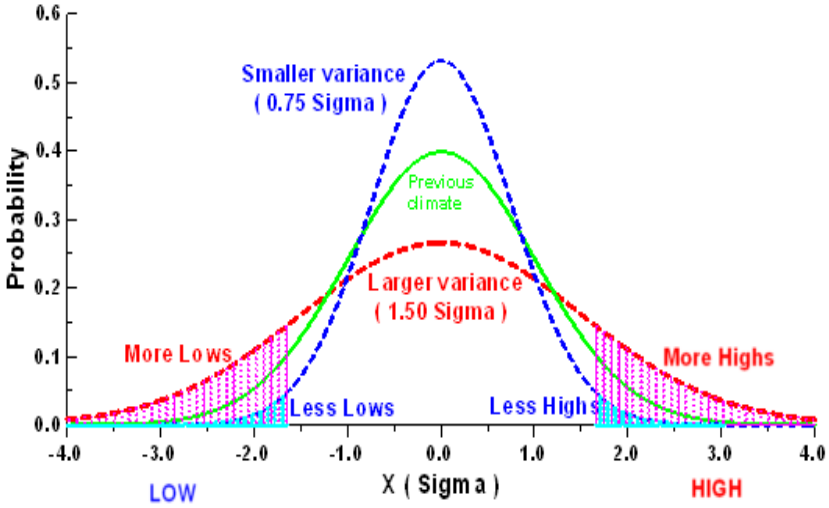

Figure 5. Probability distributions depend upon different climatologic variances (from [41]).

The IPCC [22] clarified that two statistical parameters (average and variance) should be accounted for in climate change analysis. Therefore, it might suggest, in statistics, that the standardized differences measure "net" changes relative to the anomalies, while the anomalies might be referred to "perceptual" indicators because the anomalies measure temperature variations as directly sensible for social community.

5. Conclusions

This article introduced another scanning t-test of regressive slope coefficients to directly detect change points in segment trends, along with coherency analysis. Also, the fuzzy weighted moving average (FWMA) was employed to intuitively verify the results of segment regression lines. The two algorithms were applied to the monthly temperature data of mainland China and the globe for 1901–2022.

The application results might be summarized mainly as follows:

The scanning t-test successfully detected change points of trends and fitted well with subsample data. The detected changes may be classified into two categories: on interdecadal scales and on intradecadal scales. The global warming "hiatus" contained two processes: a quick droop down from July 1998 to February 2000, and then, following a short warming up, the second process featured a warming rate slow down to nearly stable from October 2002 to June 2009 globally, but without turning to cooling. China seemed have a weaker warming slow down, but lasted longer than that of the globe.

It was a somewhat unexpected finding that the global warming rate in mainland China was lower than that of the globe in the variance-adjusted anomalies. This is contrary to the previous conclusions resulting from annual anomalies of temperature.

In statistics, we might suggest that the anomalies in $N(0,s)$ should be referred to as the "perceptual" index to be applied for comparing fluctuations in the same series or between two series with the same variance and distribution, while the standardized differences in $N(0,1)$ should be referred to a "net" indicator to compare changes/variations between two series with different variances, even in different distributions.

This article has reported statistical results only. The physical reasons need to be studied and discussed further.

Use of AI tools declaration

The author declares he has not used Artificial Intelligence (AI) tools in the creation of this article.

Acknowledgments

This work was jointly supported by the Opening Foundation of Key Laboratory of Desert and Desertification, Chinese Academy of Sciences (KLDD-2020-015), and by the Strategic Priority Research Program of the Chinese Academy of Sciences (XDA20100304). The author is grateful to Dr. Ian Harris for his kind assistance in downloading the data used in this work.

Conflict of interest

The author declares he has no any conflict of interest on this manuscript.

References

1. Varotsos CA, Efstathiou MN, Christodoulakis J (2019) Abrupt changes in global tropospheric temperature. *Atmos Res* 217: 114–119. https://doi.org/10.1016/j.atmosres.2018.11.001
2. Varotsos CA, Franzke CLE, Efstathiou MN, et al. (2014) Evidence for two abrupt warming events of SST in the last century. *Theor Appl Climatol* 116: 51–60. https://doi.org/10.1007/s00704-013-0935-8
3. Jones RN, Ricketts JH (2017) Reconciling the signal and noise of atmospheric warming on decadal timescales. *Earth Syst Dynam* 8: 177–210. https://doi.org/10.5194/esd-8-177-2017
4. Jiang J (2021) *Algorithms of the scanning tests of change-points in 4 statistic parameters and applications*, Sydney, Australia: BioByword Publishing Pty Ltd. (In Chinese).
5. Lund R, Reeves J (2002) Detection of undocumented change-points: A revision of the two-phase regression model. *J Clim* 15: 2547–2554. https://doi.org/10.1175/1520-0442(2002)015<2547:DOUCAR>2.0.CO;2
6. Jiang J (2009) Scanning detection of multi-scale significant change-points in subseries means, variances, trends and correlation. *2009 Sixth Int Conf Fuzzy Syst Knowl Discovery*, 609–613. https://doi.org/10.1109/FSKD.2009.285
7. Chen Y, Jiang J, Zhu Y, et al. (2019) Applications of multiple change-point detection to monthly streamflow and rainfall in Xijiang, Southern of China, Part II: trend and mean. *Theor Appl Climatol* 136: 489–497. https://doi.org/10.1007/s00704-018-2475-8
8. Jiang J (2023) Another scanning test of trend change in regression coefficients applied to monthly temperature on global land and sea surface. *Theor Appl Climatol*. https://doi.org/10.1007/s00704-023-04649-0
9. Yao ZS (1984) *Basic statistics in climatology*, Beijing: Sciences Press of China, 440–498. (in Chinese)
10. Bartlett MS (1966) *Stochastic processes*, 2nd ed. London: Cambridge Univeersity Press.
11. Roshydromet, Russian Federal Service for Hydrometeorology and Environmental Monitoring Climate change bulletin. 2022. (in Russian). Available from: http://www.meteorf.ru/default.aspx.
12. Liu Y, Song H, An Z, et al. (2020) Recent anthropogenic curtailing of Yellow River runoff and sediment load is unprecedented over the past 500 y. *PNAS* 117: 18251–18257. https://doi.org/10.1073/pnas.1922349117
13. Sun C, Li J, Kucharski F, et al. (2019) Recent acceleration of Arabian Sea warming induced by the Atlantic-western Pacific trans-basin multidecadal variability. *Geophys Res Lett* 46: 1662–1671. https://doi.org/10.1029/2018GL081175
14. Ding Y, Wang H (2016) Newly acquired knowledge on the scientific issues related to climate change over the recent 100 years in China. *Chin Sci Bull* 6: 1029–1041. https://doi.org/10.1360/N972015-00638
15. Ren GY, Ding YH, Zhao ZC, et al. (2012) Recent progress in studies of climate change in China. *Adv Atmos Sci* 29: 958–977.
16. Yang B, Qin C, Bräuning A, et al. (2021) Long-term decrease in Asian monsoon rainfall and abrupt climate change events over the past 6,700 years. *PNAS* 118: e210207118. https://doi.org/10.1073/pnas.2102007118
17. Jiang J (2023) A fuzzy weighted moving average to analyze actual warming. *Earth Sci Eng* 1: 43–54. https://doi.org/10.57237/j.earth.2022.01.005

18. Baas SM, Kwakernaak H (1977) Rating and ranking of multiple-aspect alternatives using fuzzy sets. *Automatica* 13: 47–58. https://doi.org/10.1016/0005-1098(77)90008-5
19. Lin KP, Hung KC (2011) An efficient fuzzy weighted average algorithm for the military UAV selecting under group decision-making. *Knowl-Based Syst* 24: 877–889. https://doi.org/10.1016/j.knosys.2011.04.002
20. Tung CT, Chu P (2014) Improved linear programming for fuzzy weighted average. *J Interdiscip Math* 17: 271–276. https://doi.org/10.1080/09720502.2013.857926
21. Morice CP, Kennedy JJ, Rayner NA, et al. (2020) An updated assessment of near-surface temperature change from 1850: the HadCRUT5 data set. *J Geophys Res Atmos* 126: e2019JD032361. https://doi.org/10.1029/2019JD032361
22. IPCC (2001) *Climate change 2001: The scientific basis. contribution of working group I to the third assessment report of the international panel on climate change*, Cambridge, UK: Cambridge University Press.
23. Harris I, Osborn TJ, Jones P, et al. (2020) Version 4 of the CRU TS monthly high-resolution gridded multivariate climate dataset. *Sci Data* 7: 109. https://doi.org/10.1038/s41597-020-0453-3
24. China Meteorological Administration, National Climate Center, China climate bulletin. 2022. Available from: http://cmdp.ncc-cma.net/cn/monitoring.htm.
25. Easterling DR, Wehner MF (2009) Is the climate warming or cooling? *Geophys Res Lett* 36: L08706. https://doi.org/10.1029/2009GL037810
26. Meehl GA, Arblaster JM, Fasullo JT, et al. (2011) Model based evidence of deep-ocean heat uptake during surface –temperature hiatus period. *Nature Clim Change* 1: 360–364. https://doi.org/10.1038/nclimate1229
27. Estrada F, Perron P, Martinez-Lopez B (2013) Statistically derived contributions of diverse human influences to twentieth-century temperature change. *Nature Geosci* 6: 1050–1055.
28. Guemas V, Doblas-Reyes FJ, Andreu-Burillo I, et al. (2013) Retrospective prediction of the global warming slowdown in the past decade. *Nature Clim Change* 3: 649–653. https://doi.org/10.1038/nclimate1863
29. Hawkins E, Edwards T, McNeall D (2014) Pause for thought. *Nature Clim Change* 4: 154–156. https://doi.org/10.1038/nclimate2150
30. England MH, McGregpr S, Spance P, et al. (2014) Recent intensification of wind-driven circulation in the pacific and the warming hiatus. *Nature Clim Change* 4: 222–227. https://doi.org/10.1038/nclimate2106
31. Chen X, Tung K (2014) Varying planetary heat sink led to global-warming slowdown and acceleration. *Science* 345: 897–903. https://doi.org/10.1126/science.1254937
32. Clement A, DiNezio P (2014) The tropical Pacific Ocean—Back in the driver's seat? *Science* 343: 976–978. https://doi.org/10.1126/science.1248115
33. Trenberth KE, Fasullo JT, Branstator G, et al. (2014) Seasonal aspects of the recent pause in surface warming. *Nature Clim Change* 4: 911–916. https://doi.org/10.1038/nclimate2341
34. Trenberth KE (2015) Has there been a hiatus? *Science* 349: 691–692. https://doi.org/10.1126/science.aac9225
35. Karl TR, Arguez A, Huang B (2015) Possible artifacts of data biases in the recent global surface warming hiatus. *Science* 348: 1469–1472. https://doi.org/10.1126/science.aaa5632
36. Lewandowsky S, Risbey J, Oreskes N (2015) On the definition and identifiability of the alleged "hiatus" in global warming. *Sci Rep* 5: 16784. https://doi.org/10.1038/srep16784

37. Lewandowsky S, Risbey J, Oreskes N (2016) The “pause” in global warming: Turning a routine fluctuation into a problem for science. *Bull Amer Meteor Soc* 97: 723–733. https://doi.org/10.1175/BAMS-D-14-00106.1
38. Sun X, Ren GY, Xu W, et al. (2017) Global land-surface air temperature change based on the new CMA GLSAT data set. *Sci Bull* 62: 236–238. https://doi.org/10.1016/j.scib.2017.01.017
39. Luu QH, Wu Q, Tkalich P, et al. (2018) Global mean sea level rise during the recent warming hiatus from satellite-based data. *Remote Sensing Lett* 9: 497–506. https://doi.org/10.1080/2150704X.2018.1437291
40. Jones PD, Lister DH, Osborn TJ, et al. (2012) Hemispheric and large-scale land surface air temperature variations: an extensive revision and an update to 2010. *J Geophys Res* 117: D05127. https://doi.org/10.1029/2011JD017139
41. Jiang J, Gu X, Timonen M, et al. (2015) Chapter 5: Significant change-points of subperiod levels in tree-ring chronologies as indications of climate changes. *Adv Environ Res* 37: 109–146.

AIMS Press